Published in final edited form as:
J Phys Chem B. 2010 March 4; 114(8): 2944–2953. doi:10.1021/jp909531s.

Water induced relaxation of a degenerate vibration of guanidinium using 2D IR echo spectroscopy

Dmitriy Yu. Vorobyev[1], **Chun-Hung Kuo**[1,§], **Daniel G. Kuroda**[1], **J. Nathan Scott**[2], **Jane M. Vanderkooi**[2], and **Robin M. Hochstrasser**[1,*]

[1]Department of Chemistry, University of Pennsylvania, Philadelphia, PA 19104, USA

[2]Department of Biochemistry and Biophysics, University of Pennsylvania, Philadelphia, PA 19104, USA

[§]Technology and Application Center, Newport Corporation, 1791 Deere Ave., Irvine, CA 92606, USA

Abstract

The nearly degenerate asymmetric stretch vibrations near 1600 cm^{-1} of the guanidinium cation in D-glycerol/D_2O mixtures having different viscosity were studied by 2D IR photon echo spectroscopy. The polarization dependent photon echo signal shows two separate frequency distributions in the 2D spectrum in D_2O, even though only one band is evident from inspection of the linear FTIR spectrum. The split components are more clearly seen at higher viscosity. The interactions with solvent induce energy transfer between the degenerate component modes on the time scale of 0.5 ps. The energy transfer between modes is directly observed in 2D IR and distinguished by the waiting time dependence of the cross peaks from the transfers between threefold symmetric configurations of the distorted ion and solvent. The 2D IR analysis carried out for various polarization conditions required specification of frequency-frequency auto- and cross- correlation functions for the degenerate components.

Keywords

Ultrafast 2D IR spectroscopy; guanidinium chloride; photon-echo; population transfer; coherence transfer

INTRODUCTION

It remains an outstanding challenge to find a microscopic interpretation of the mechanism whereby Guanidinium chloride (GdmCl) denatures proteins. It readily unfolds almost all proteins, often at low GdmCl concentrations[1–3]. Two perspectives have been proposed for the protein denaturation by the amphiphillic ion Gdm^+: one invokes the direct interaction of Gdm^+ with nonpolar groups of proteins[4–6], and the other gives a key role to changes in the water structure induced by Gdm^+[7]. Therefore it is of value to design experiments that probe this ion along with its associated water structure and accompanying dynamics. In the present experiment 2D IR (two dimensional infrared) spectroscopy is used to provide new information regarding the structural and dynamical characteristics of Gdm^+ and its associated water.

*To whom correspondence should be addressed. hochstra@sas.upenn.edu. Phone: 215-898-8410. Fax: 215-898-0590.

The isolated Gdm^+ ion has D3 symmetry with the C and N atoms on the plane perpendicular to a three fold symmetry axis[8] as shown on Figure 1. Each of the NH2 group planes makes an angle ~ 12° with the CN_3 plane. The isolated ion has a degenerate mode around 1600 cm^{-1} corresponding to a combined CN_3 asymmetric stretch and NH_2 scissors motions. The symmetric stretch of CN_3 is around 1000 cm^{-1}. Asymmetric stretch mode has a large (ca. 0.5D) transition dipole[9]. Therefore the IR band of isolated Gdm^+ at ca. 1600 cm^{-1} should correspond to two transitions at the same frequency having orthogonal transition dipole directions. In a solvent at each instant these modes become distinguishable and the transition dipole directions become well defined in the molecular frame. The 2D IR methods can probe the structure distributions of solvent associated ions and also the dynamics of any structural relaxations. By accessing both structural and dynamical features in a single experiment 2D IR[10] can provide the transition dipole reorientational motions, intermode coupling and time dependent frequencies of each of the vibrational transitions on the ultrafast time scales commensurate with expectations for H-bond dynamics in aqueous ionic solutions as recently demonstrated for small ions[11–13].

There is a significant literature on the linear IR and two dimensional vibrational echo spectroscopy of coupled anharmonic oscillators[13–21]. They are modeled by two zero-order modes whose V=0→V=1 transitions may be chosen as nearly degenerate, such as in a symmetric dimer[16] or a dipeptide[22, 23], but whose eigenmodes are split by virtue of the term in the Hamiltonian that couples the two modes. The coupling for a pair of anharmonic oscillators represents an excitation exchange interaction which is often approximated for strong transitions as a dipole-dipole interaction. The existence of the coupling causes the eigenmodes to become linear combinations (that is, excitons) of the zero order modes. This is a fundamentally different situation than expected for a delocalized degenerate mode of a three-fold or higher symmetry system. In this case the vibrational eigenmodes have the same frequency, or they have nearly the same frequency if the molecule is in a solvent whose instantaneous structures might slightly break the exact symmetry. In the three-fold symmetry, the coupling of the vibrational and rotational angular momenta (Coriolis coupling) will cause one degenerate component to transfer into the other and the degenerate levels to split. If the solvent interactions strongly quench these angular momenta, the two modes may still mix and split as a result of them having different chemical interactions with surrounding solvent molecules. The splitting need not be caused by an excitation exchange interaction and in a first approximation the two components of the split degeneracy are still the same delocalized vibrational eigenmodes. Thus we see that the degenerate transition presents opportunities to evaluate the solvent interactions from a perspective that differs completely from the spectra of coupled anharmonic oscillators. Nevertheless the coupling to solvent can induce energy transfer between the nearly degenerate modes which can be detected by anisotropy measurements and by 2D IR[24–26] because the nearly degenerate modes have nearly perpendicular transition dipoles. The energy transfer is expected to induce cross peaks in the 2D IR spectra[25–27] allowing the transfer kinetics to be defined and evaluated.

Recent pump-probe measurements of the anisotropy for the 1600 cm^{-1} transition of Gdm^+ have revealed sub-picosecond solvent induced transfers between the two nearly degenerate components. Intermode energy transfer has been invoked to explain anisotropy decays in a number of other examples[24, 28, 29]. These include CN vibrations of hexacyanides[24] and CO vibrations of hexacarbonyls[28, 29] for which the degenerate states can be described by the superpositions of modes that are localized on symmetrically placed CN or CO groups. The relaxation kinetics is then analogous to the relaxation of Frenkel excitons. The present example of Gdm^+ is conceptually different in that the relaxation of Gdm^+ is intrinsically related to solvent induced mixing of the two nearly degenerate, *delocalized* vibrations that are not intrinsically exciton-like. In the present paper we investigate these solvent effects through their influence on the vibrational frequency distributions and dynamics for this nearly degenerate

pair of Gdm^+ transitions at ca. 1600 cm^{-1} using polarization dependent femtosecond 2D IR photon echo and heterodyned transient grating methods.

EXPERIMENTAL METHODS

Sample Preparation

The guanidinium chloride purchased from Sigma-Aldrich (http://www.sigmaaldrich.com) is fully deuterated ($C(ND_2)_3^+$, $DGdm^+$ and dissolved in D_2O. Deuteration prevents the spectral overlapping of degenerate mode of $DGdm^+$ at ca. 1600 cm^{-1} with OH bending. The salt was completely deuterated by successive dissolution in excess D_2O followed by lyophilization. Samples were held between two CaF_2 plates separated by a 12 micron spacer. The use of concentrations less than ~0.2 M ensured that the $DGdm^+$ ions were not aggregated[30]. D-glycerol/D_2O, 59% (by weight) with viscosity 10 cP[31] at 295K were also used in the experiments. Sample without spacer and with the concentration of 1.5 M was used in transient grating experiment.

Linear FTIR spectroscopy

Linear FTIR spectra were obtained with Thermo Nicolet 6700 FTIR spectrometer with 0.5 cm^{-1} resolution.

2D IR photon-echo experiment

A detailed description of the 2D IR photon-echo experiment and data processing can be found elsewhere[13, 32]. Here, we employed Fourier-transform limited 75 fs pulses with center frequencies at 1600 cm^{-1}. Three of these pulses each with energy 400 nJ and wave vectors $\vec{k}_1$, $\vec{k}_2$ and $\vec{k}_3$ were incident on the sample. The phase-matched signal at wave vector $-\vec{k}_1+\vec{k}_2+\vec{k}_3$ was detected by heterodyning it with a local oscillator pulse that always preceded the signal pulse by a fixed interval of ~1.0 ps. The interval between pulses 1 and 2 is denoted as τ, that between 2 and 3 as T, and that between 3 and the detected signal as t. In the rephasing (nonrephasing) sequence the beam $\vec{k}_1$ arrives earlier (later) than $\vec{k}_2$ by an amount τ. The signal and local oscillator pulses were combined at the focal plane of a monochromator having a 64-element MCT array detector (IR Associates, Inc.). The raw data collected using this method was a function $S(\tau,\lambda_t,T)$ of the two time intervals and wavelength. Fourier transformation along τ and transformation of λ_t to ω_t generate the two-dimensional spectra $\tilde{S}(\omega_\tau,\omega_t,T)$ for each population interval T. To obtain absorptive spectra, the rephasing and nonrephasing were added at each value of T. For polarization dependent echo experiments the incident and local oscillator pulses passed through polarizers to produce either same polarization for all pulses and the XXXX tensor signal or perpendicular polarization of $\left(\vec{k}_1,\vec{k}_2\right)$ and $\left(\vec{k}_3,\vec{k}_{LO}\right)$ pulses corresponding to the XXYY tensor. In the transient grating experiment the XYYX tensor was also investigated. Polarization dependent heterodyned transient grating data (TG) were obtained by scanning T at zero delay between first two interactions, $\vec{k}_1$ and $\vec{k}_2$.

EXPERIMENTAL RESULTS

The FTIR spectra of $DGdm^+$ in the 1500 ~ 1700 cm^{-1} region in different solvents are shown in Figure 2. This spectral region is presumed to incorporate the degenerate asymmetric stretch mode of the CN_3 group of $DGdm^+$. The FTIR spectrum of $DGdm^+$ in D_2O has one symmetric peak centered at 1599 cm^{-1} (ε = 868±8 M^{-1} cm^{-1}). The change of solvent to a glycerol/water mixture leads to clear splitting of this band into two components: the first centered at 1600 cm^{-1} (ε = 831 ± 65 M^{-1} cm^{-1}) and the second as a shoulder at 1590 cm^{-1}.

The polarization dependent absorptive 2D IR spectra of DGdmCl in D_2O are shown in Figure 3 while those of DGdmCl in D-glycerol/D_2O are shown in Figure 4. In both these Figures the data are shown in the left-hand columns: the right-hand columns are simulations to be discussed later in the paper. The details of the 2D IR data in Figures 3 and 4 show conclusively that the 1600 cm^{-1} band of $DGdm^+$ consists of two identifiable frequency distributions peaked at different locations on the diagonal of the 2D IR spectra. It is also clear that there are cross peaks connecting these two diagonal transitions. The specific features of these 2D IR spectra, pertaining mainly to the V=0→V=1 contribution, which is shown in the blue in Figures 3 and 4, are summarized in the following description.

The XXXX polarization 2D IR spectra in Figures 3.1a and 4.1a are both elongated along the diagonal at waiting time T = 0 ps. They both show multiply peaked distributions that are most apparent for the D-glycerol/D_2O spectra. For the D_2O case, the trace of the 2D spectral signal along the diagonal line drawn in Figure 3, presented in the upper panel of Figure 3.1a, shows the asymmetry that indicates of multiple states. In D_2O the peaks appear at ω_τ = 1600 cm^{-1} and ~1590 cm^{-1}. In D-glycerol/D_2O (Figure 4) they are readily identified at ω_τ =1586 cm^{-1} and 1602 cm^{-1}. These doublet spectra in D_2O merge into a single peak with central frequency ω_τ = 1598 cm^{-1} after a waiting time of 2 ps. The relaxed spectrum resembles an almost upright ellipse with its major axis along the coherence frequency axis ω_τ. At a waiting time T=2 ps the two diagonal peaks of the 59% D-glycerol/D_2O sample are shifted to ω_τ =1587 cm^{-1} and 1601 cm^{-1} and the lower frequency peak has decreased in intensity. This decrease combined with the increase in cross peak intensity causes the spectrum to appear more upright, as in Figures 3.1b and 4.1b. The term upright signifies that the 2D IR spectrum not tilted from the orthogonal frequency axes. The analysis given later will show that the spectral evolutions of the two samples are quite similar although the increased splitting in glycerol/D_2O makes it more readily visualizable. The lower frequency peak appears to decrease significantly with increasing T delay. In both solvents this decrease is accounted for by the overlap of the diagonal negative peak with the positive component of the cross peak. The XXYY 2D IR spectrum of $DGdm^+$ in D_2O at T=0 ps shows (see Figure 3) some elongation along the diagonal but it is more upright than the corresponding XXXX spectrum. The significant differences between the XXXX and XXYY signals, evident even at equivalent waiting times, are best visualized by comparing Figures 3.1a with 3.1c or 4.1a with 4.1c. The D_2O sample shows only one peak at ω_τ =1599 cm^{-1} for T = 0 but the spectrum evolves to have a distinctly upright shape at T = 2 ps. In D-glycerol/D_2O, shown in Figure 4, cross peaks linking the two diagonal peaks are clearly seen along with two diagonal peaks at ω_τ = 1585 cm^{-1} and 1601 cm^{-1}. At T=2 ps a lower frequency diagonal peak is no longer present, and an upright spectrum is seen that has two peaks along the coherence frequency ω_τ, at 1598 cm^{-1} and 1590 cm^{-1} as shown in Figure 4.

The heterodyned TG signals, recorded at the maximum of the photoinduced absorption are presented in Figure 5(a). They permit a direct comparison of the three tensor components. The XXXX and XXYY signals provide the same information as the polarization dependent pump-probe experiment. The T_1 lifetime is obtained from the time evolution of the isotropic signal (XXXX+2XXYY) which, in combination with XXXX−XXYY, yields the anisotropy. The T_1 lifetime of 1.8 ps obtained from the TG experiment is in excellent agreement with that obtained from pump-probe data[30]. The anisotropy presented on Figure 5(b) has a double exponential decay with time constants 0.43±0.07 ps and 13±7 ps and amplitudes 0.34±0.05 and 0.07±0.01. The parameters of the anisotropy agree reasonably with the more accurate pump-probe measurements[30]. The tensor XYYX decays very quickly compared with the other components and its evolution coincides with the rise of XXYY signal. The XYYX tensor decay could be reasonably fit with one exponential decay function with a time constant of 0.38 ps comparable with the fast decay of the anisotropy. The slow decay part of the anisotropy is too small to measure definitively in the heterodyned TG experiment that we performed.

DISCUSSION

The absorptive 2D IR spectra [XXXX, T = 0] in D_2O in Figure 3 clearly demonstrate that the transition at ca. 1600 cm^{-1}, which shows a single band in FTIR, is composed of a multiple peaked frequency distribution along the diagonal of the 2D IR spectra, having at least two well-defined peaks. The spectra have an upright shape in D-glycerol/D_2O and in neat D_2O indicating that there is a cross peak between the two peaks of the distribution that is polarization sensitive. In D-glycerol/D_2O the cross peak is more readily visualized (see Figure 4) and it is evident by inspection that the relative amplitude of the cross peak at ω_τ =1601 cm^{-1} increases compared with the diagonal peak at 1601 cm^{-1} as T increases. The increase of cross peak amplitude with increasing T tends to make the spectra appear more upright and elongated along ω_τ for all solvents and polarization conditions.

The time scale of the cross peak evolution was derived from the relative amplitude of the cross peak compared with one of the diagonal peaks. Slices along ω_τ at ω_τ =1601 cm^{-1} (refer to Figure 4) were used to obtain the T dependences of the ratios shown in Figure 6 of signal amplitudes at ω_τ =1585 cm^{-1} and ω_τ =1601 cm^{-1}, for XXYY and XXXX polarizations in D-glycerol/D_2O. The exponential fit of the ratios gives a time constant of 550±70 fs for cross peak growth. This manner of analysis removes the effect of population relaxation which causes the overall signal to decay during the T period. The T dependence and polarization dependence of cross peak amplitude immediately suggests there is energy transfer between the two nearly degenerate asymmetric stretches[25, 26].

The decay of the transient grating signal includes contributions from rotational diffusion and any processes leading to reorientation of the transition dipole moments. Rotational diffusion of the molecule with two perpendicular transitions in a spherical molecule approximation would provide a decay of XXXX and XXYY components to a constant value and of the XYYX component to zero, as is readily seen from orientational averaging for each component[33]. The ultrafast decay of the XYYX component occurs on a time scale much faster than characteristic times in rotational diffusion 1/6D and 1/2D. Moreover, the time scales of the XYYX decay and cross peak growth in 2D IR spectra are very similar, suggesting that the two effects have the same origin, namely energy transfer between two nearly degenerate modes which leads to reorientation of the two transition dipole moments. These cross peak dynamics and fast decay of the XYYX component of the TG signal are occurring on the time scale of recently reported pump-probe anisotropy decay for $DGdm^+$ in D_2O and in D-glycerol/D_2O[30]

The dephasing and energy transfer parameters obtained from the 2D IR experiment/simulation, described below, are considerably more accurate than those from the TG.

2D IR PHOTON-ECHO SIMULATION

2D IR photon echo spectra for dilute solutions of $DGdm^+$ were simulated by assuming a model consisting of the six states shown in Figure 7 and the response functions illustrated by the pathways in Figure 8. In the model there are two one quantum states ($1\equiv|10\rangle$ and $2\equiv|01\rangle$) which are the components of the degenerate level. The transition dipole moments to these states from $|00\rangle$ are assumed to be perpendicular. There are three two quanta states ($1+2\equiv|11\rangle$, $2+2\equiv|02\rangle$, $1+1\equiv|20\rangle$). The frequencies of the $|01\rangle\rightarrow|02\rangle$ or $|10\rangle\rightarrow|20\rangle$ transitions are each downshifted by Δ from the fundamental frequency. The $|11\rangle$ state is downshifted by Δ_c from the sum of the two fundamental frequencies. This choice of system eigenstates to describe the solvent induced dynamics of the degenerate manifold of states has been discussed in detail previously[30]. The simulation is based on response functions given in reference[34] and assuming delta function excitation pulses. The relevant diagrams are shown in Figure 8 (rows 1–3). The dephasing dynamics are discussed below.

We first consider the fast cross peak growth shown in Figure 6. The D_3 point symmetry of gas phase $DGdm^+$ will be broken by asymmetric solvent interactions at any instant in the solution phase. The distorted structure that arises must have three equivalent orientations in space that carry with them three solvation shell structures: these configurations are labeled as A_1, A_2 and A_3. For these three configurations the ion normal modes for different molecules in the sample would be identical except for a three-fold rotation in space. The IR transition dipole moments would be rotated by $\pm 2\pi/3$ in the plane of an ion. If an A_1 configuration were excited by a short pulse, the redistribution of water molecules in the solvation shell and adjustments of the coupling of solvent to the ion would cause a transfer into the A_2 or A_3 configuration. Even in the absence of overall molecular rotation, at long delays after excitation of A_1 the three configurations will have appeared an equal number of times, and would not be distinguishable. We will show that this process is slower than energy transfer. The former incorporated into the simulation through a simplified kinetics scheme that involves one rate coefficient, k_s, connecting any pair of configurations A_1, A_2 and A_3. These $2\pi/3$ flips of the transition dipole moment direction cause a loss of anisotropy on the time scale $(3k_s)^{-1}$ In the 2D spectrum the time dependence of both the diagonal and cross peaks are sensitive to this effect.

The decay of anisotropy and cross peak growth in the 2D IR echo experiment will also be modified by solvent induced energy transfer between the two split degenerate components of any one of the three configurations A_1–A_3, which will cause stochastic jumps of $\pi / 2$ in the transition dipole directions.

The present analysis incorporates all the response functions for the nearly degenerate oscillator and it is assumed that the rate constants for energy transfer and coherence transfer during the T period are equal. This latter idea is based on a highly simplified picture of the system-bath interaction where the solvent bath is not influenced by the vibrational motions of the $DGdm^+$ system. As mentioned in an earlier paper[30], the system-bath interaction V is considered to depend on the normal modes Q_1 and Q_2 of the $DGdm^+$ degenerate state, and on the coordinates, q, of the bath:

$$V = V(q, Q) = \sum_{i=1,2} V_i(q)\, Q_i + \sum_{i,j=1,2} V_{ij}(q)\, Q_i Q_j + \ldots \tag{1}$$

The equation of motion describing the dynamics of the reduced density matrix elements, in the basis of the six state model defined above, has the following form in each of the τ, T and t periods of photon echo experiment:

$$\dot{\rho}_{ij}(t) = \sum_{k,l} e^{i(\omega_{ij}-\omega_{kl})t} R_{ij;kl}\rho_{kl}(t) \tag{2}$$

where R is a Redfield matrix[35, 36] and $|\omega_{ij}-\omega_{kl}| \square \Delta t^{-1}$, where Δt is a measure of the evolution time of the system. Subpicosecond evolution times and near degeneracy results in many pairs of states chosen from the six state model being able to satisfy this inequality and so many density matrix elements need to be considered in the simulation. It was shown in earlier work that coherence transfer in the t period does not contribute much to the dynamics[30] so here, we consider only coherence transfer during the T period during which time population transfer also occurs. In the simplified analysis the bath is not influenced by the solute, and it is characterized by a spectral density g(ω), so the rate coefficient for population transfer ($\pi / 2$ flips) between degenerate components 1 and 2 and for coherence transfer are defined as:

$$k_{et}=k_{11->22}=k_{12->21}=\frac{|V_{12}|^2}{\hbar^2}g(0) \tag{3}$$

These rate coefficients are the Redfield elements:

$$R_{2211}=k_{11->22}=\frac{2\pi}{\hbar^2}\sum_r P_r\sum_s|\langle s,2|V|r,1\rangle|^2\delta(\omega_{rs}-\omega_{12}) \tag{4}$$

$$R_{1112}=k_{12->21}=\frac{2\pi}{\hbar^2}\sum_r P_r\sum_s\langle s,2|V|r,1\rangle\langle r,2|V|s,1\rangle\delta(\omega_{rs}-\omega_{21}) \tag{5}$$

where s and r represent the eigenstates of the bath and P_r is the Boltzmann factor for state r of the bath. Equations (3) – ([5]) are readily obtained from the Redfield Equation[36] for $R_{\alpha\beta\gamma\delta}$. In the present situation since the degeneracies have small splittings we assume that $\omega_{12} \approx \omega_{21} \approx 0$. The equality of $k_{11\rightarrow22}$ and $k_{12\rightarrow21}$ in the simple model is readily verified from properties of V=0 and V=1 of harmonic oscillators. It is noted that the energy transfer and the coherence transfer defined by Equation (3) both depend on the variance of the fluctuations of the bath, $g(0)$. As mentioned above, the exchanges of the coherences ρ_{01} and ρ_{02} created by the first pulse are considered to be slower because the states 1 and 2 are eigenmodes of the system and the exchange between ρ_{01} and ρ_{02} would appear to require fluctuation of the bath on the time scale of the fundamental transition frequencies, a result which arises from the restricted Redfield model described above. This coherence transfer depends on $g(\omega_{01})$, which is likely to be much less than $g(0)$ when $\hbar\omega_{10} >> K_BT$, which is certainly the case for a high frequency vibration. For this reason the ρ_{01} , ρ_{02} exchange during τ is neglected. Our previous experiments on the pump-probe analysis

As already mentioned, the signal will depend on the 2π / 3 flips between configurations. However, since this process involves significant solvent reconfiguration it would be expected to slow down considerably at higher viscosities. The experiments in D_2O and glycerol/water mixtures give quite similar results in regard to time dependence as shown by comparing Figure 3 and 4 at 2 ps. These results indicate that the effect of viscosity on the cross peak dynamics is not large, suggesting that the π / 2 flips are the dominant effect. The following analysis, which incorporates both processes clearly indicates that energy transfer is indeed the dominant mechanism for reorienting the transition dipoles.

To account for the energy transfer in the simulation the rephasing and nonrephasing pathways shown in Figure 8 (rows 4, 5) were incorporated. The main point of these diagrams is that the evolution involves a spontaneous component during T which is represented in the diagrams as the dashed line. This process can cause a population that was driven into one state to be detected through another state into which it spontaneously flows. Similarly it can result in a coherence during T being transformed into its conjugate with a rate described by Equation (5). During the T period the system is assumed to undergo kinetics induced by the system - bath interaction which is incorporated through a multiplicative factor. This factor is $\frac{1}{2}\left(1-e^{-2k_{et}T}\right)$ for the diagrams in rows (4) and (5) which are those experiencing population or coherence transfer. The probabilities for these diagrams undergoes growth from zero to a limiting contribution of 50%. The corresponding diagrams in rows (1) – (3), which are those not undergoing transfers, are multiplied by a factor $\frac{1}{2}\left(1+e^{-2k_{et}T}\right)$. They undergo decay to the same 50% limit. Each

diagram in rows (1) to (3) excluding the ground state bleaching terms, has a partner in rows (4) and (5). The rate coefficient k_{et} is defined in Equation (3). The influence of the diagrams in rows (4) and (5) on the signal vanishes when $k_{et}T \ll 1$.

The relaxation parameters included population lifetimes and dephasing processes. The T_1 lifetimes of the states obtained from magic angle pump-probe measurements were 1.82 ps and 2.44 ps for $DGdm^+$ in D_2O and in the 59%D-glycerol/D_2O mixture respectively[30]. The population lifetimes for the two nearly degenerate states were assumed to be equal and a harmonic approximation was used to define the lifetimes of doubly excited states. The pure dephasing was incorporated through integrated relaxation functions $g_{11}(t)$, $g_{22}(t)$ and $g_{12}(t)$ with parameters as described below. Orientational factors for two perpendicular transition dipole moments in the approximation of a spherical diffuser were employed in the simulation[33]. A path such as the first diagram in line 4 of Figure 8 involves energy transfer, and its orientational factor is taken from column iijj of Table 1a since the first two field interactions are with one mode (i) and second two are with the other (j). The 2π / 3 flip contributes to all diagrams. Its kinetic factors are chosen as $\frac{1}{3}\left(1+2e^{-3k_sT}\right)$ for the starting configuration, say A_1, and $\frac{1}{3}\left(1-e^{-3k_sT}\right)$ for the other two configurations. Thus, for each diagram the orientational coefficient $\langle a_k b_l c_m d_n \rangle$ is replaced by:

$$\begin{aligned}&\frac{1}{3}\left(1+2e^{-3k_sT}\right)\left\langle a_k^{A_1} b_l^{A_1} c_m^{A_1} d_n^{A_1}\right\rangle\\&\quad+\frac{1}{3}\left(1-e^{-3k_sT}\right)\left\langle a_k^{A_1} b_l^{A_1} c_m^{A_2} d_n^{A_2}\right\rangle\\&\quad+\frac{1}{3}\left(1-e^{-3k_sT}\right)\left\langle a_k^{A_1} b_l^{A_1} c_m^{A_3} d_n^{A_3}\right\rangle\end{aligned} \tag{12}$$

where superscripts A_1, A_2, A_3 indicate which of the three configurations interacts with the excitation field. Values for $\left\langle a_k^{A_1} b_l^{A_1} c_m^{A_2} d_n^{A_2}\right\rangle$ and $\left\langle a_k^{A_1} b_l^{A_1} c_m^{A_3} d_n^{A_3}\right\rangle$ are given in Table 1b.

The 2D IR spectra of the split components of the degenerate state are congested so it is useful to visualize them as a function of T for the two components artificially separated in frequency, but otherwise with parameters for the degenerate transitions, as shown in Figure 9 in which spectra are simulated for T=0 and also for T=2 ps. The 2 ps panels are for three different relaxation mechanisms: In the first column of panels (2a and 2b) only the spectral diffusion and T_1 processes are incorporated. In the second (3a and 3b) the coupling to induce π / 2 jumps is added. The third panels (4a and 4b) include spectral diffusion, T_1 processes and 2π / 3 flips. Even without detailed processing the simulated spectra show clearly that the cross peak growth is completely different for the different mechanisms. The plots of ratios between cross peak and diagonal peak signals for the two mechanisms are shown on Figure 10. Comparisons with the experimental data for D-glycerol/D_2O shown in Figure 6 show clearly that the energy transfer model agrees well with experiment and must be the dominant mechanism for cross peak growth in the D-glycerol/D_2O mixture. The data show that k_{et} must be much greater than k_s.

Simulated 2D IR spectra for different polarization conditions are shown on Figure 3 and Figure 4 using parameters given in Table 2. The central frequencies, ω_1 and ω_2, of two modes, their transition dipole moments, μ_1 and μ_2, the parameters for the autocorrelation and crosscorrelation functions and the rotational diffusion coefficients were chosen to satisfy both the linear FTIR and the 2D IR spectra. Simulated linear FTIR spectra are presented on Figure 2 with curves drawn by circles. The energy transfer rate coefficients were k_{et}=0.53 ps^{-1} in neat D_2O and k_{et}=0.71 ps^{-1} in D-glycerol/D_2O[30]. The simulation incorporated rotational diffusion

coefficients of $3.3*10^{10}$ s^{-1} for D_2O and $0.33*10^{10}$ s^{-1} for D-glycerol/D_2O[30]. Figures 3, 2a and 2c show the simulated spectra for XXXX and XXYY polarizations where the main features of the experiment (Figure 3, 1a and 1c) are captured: the XXYY spectrum is proven to be upright (i.e. not tilted from the frequency axes) because of the presence of underlying cross peaks. The simulations in 2a and 2c of Figure 4 reproduce all the main features of the experiment at T=0. The T-dependent growth of the cross peak is also reproduced by the simulation for both samples. In the more viscous solvent, where two bands are more separated in frequency and have different intensities the agreement between the simulation and experiment is more easily visualized. In the simulations the dephasing contributions to the responses were treated differently for different diagrams.

The vibrational frequency autocorrelation function C(t) required for the diagrams in line (1) of Figure 8 was assumed for each of the transitions to be the same sum of a homogenous part γ and a Kubo function, namely: $C(t) = 2\gamma\delta(t) + \Delta^2 e^{-t/\tau}$, where the product τΔ is approximately equal to or greater than unity. The diagrams in line (2) involve pumping one transition and probing the other so they require a cross correlation between the two frequency distributions. The homogeneous parts of these transitions are considered, by definition, to be completely uncorrelated so that a cross-correlation function $C_{12}(t)$ of the two vibrational frequencies was incorporated in the approximate form: $C_{12}(t) = f\Delta^2 e^{-t/\tau}$ where *f* is a correlation coefficient that was allowed to vary between 1 and -1. The diagrams in line (2) and (3) were evaluated by using these same auto and cross correlation functions. With these definitions the decay during T depends on the homogeneous relaxation parameter g only when there is a 1-2-coherence, as in the diagrams in row (3) of Figure 8, otherwise the homogeneous dephasing has no influence during T. The integrated relaxation parameters (the g(t) functions [35]) have been set down in detail elsewhere [34] and need not be reproduced here. In the initial fitting the pairs of and t parameters of the auto and cross-correlation functions were allowed to vary independently but they consistently emerged as being approximately equal therefore in the fits shown in this paper they were assumed to be equal and only one pair of values of = 2 ps^{-1} and t = 1.13*ps* for water and = 1.45ps^{-1} and t = 1.5*ps* for D-glycerol/D_2O are quoted. The values of the homogeneous dephasing rates were found to be g = 0.84 ps^{-1} for the D_2O solvent and g = 0.51 ps^{-1} for the D-glycerol/D_2O mixture. The picosecond correlation time t is attributed to the reconfiguration of the local water structures involving the ND_2 groups of $DGdm^+$ as will be discussed in next section. The cross correlation function of the split component frequencies presented on Figure 3 and 4 utilizes a correlation factor value *f* = -1 for both solvents. The equality of the cross-correlation and auto-correlation times indicates that the same solvent reconfigurations are responsible for both processes. The response functions for the $DGdm^+$ transitions in D_2O and in D-glycerol/D_2O solvents incorporate quite similar frequency-frequency auto- and cross-correlation functions. The visual difference in the experimental results for the two solvents shown in Figures 3 and 4 originates from differences in three parameters: the dephasing contributions from population lifetime and reorientation; the solvent dependent splitting of two frequency distributions; and the relative strengths of the two transition dipole moments.

The simulation showed that the shape of the 2D IR spectra is very sensitive to the correlation between the frequency distributions of the two modes. A negative correlation is required to reproduce the shape of the absorptive spectra for XXYY experiment at T = 0 for $DGdm^+$ in D_2O and in D-glycerol/D_2O shown in Figure 3 and 4. This shape arises because the cross peak tilted toward the antidiagonal direction. This anticorrelation is consistent with the notion that the solvent forces that are splitting the degeneracy tend to push the component states apart. In both solvents the frequencies of the two component modes, w_1 and w_2, are well separated with the average values of w_2-w_1 being 10.6 cm^{-1} for D_2O and 14.2 cm^{-1} in D-glycerol/D_2O. These splittings are readily accounted for by water H-bonding not only breaking the symmetry but distorting the -ND_2 groups as discussed below. In D-glycerol/D_2O the diagonal

anharmonicities aising from the fits are 18±1 cm^{-1} for the lower frequency transition and 11 ±1 cm^{-1} for the higher frequency mode. These values are significantly different.

RELATIONSHIP OF 2D IR TO STRUCTURAL DYNAMICS

The influence of water interactions with Gdm^+ on the frequency fluctuation of the nearly degenerate asymmetric stretches was first addressed by classical MD simulation. The simulation was performed with the NAMD package [37] using a box with a side of 30 Å containing 816 TIP3P waters and one Gdm+ cation. Parameters for Gdm^+ were from the topology file for proteins in CHARMM22. A 1 ns duration trajectory was simulated with 20 fs step. The fluctuation of the NH_2 groups was analyzed by means of the fluctuation of the angle (φ) between CN bond and the plane containing a N and two H atoms of a selected NH_2 group.

Radial distribution functions $g_{COw}(r)$ for C_{Gdm+}-Owater and $g_{NOw}(r)$ for N_{Gdm+}-Owater are presented on Figure 11a. The three nitrogens are equivalent and data for only one of them are shown. The positions of the first peak on the distributions, 2.9 Å for $g_{NOw}(r)$ and 3.8 Å for $g_{COw}(r)$, clearly indicate the amphiphilicity of the Gdm^+: there is a significant lack of the water density immediately above and below Gdm^+ plane in comparison with the water density around NH_2 groups. Water molecules cannot approach the ion perpendicular to its plane and achieve normal H-bond separations from the carbon to oxygens of water. So the ion has a hydrophobic shield which only allows amphiphilic character towards water molecules around the perimeter of the ion that are approaching in directions that project significantly onto the plane of the CN_3 group.

The MD simulation shows that reconfiguration of the H-bonded water molecules around the perimeter leads to significant variations in the -NH_2 group geometries. The angle j was chosen to characterize the fluctuation of NH_2 groups. A semi-quantitative picture of the time evolution of the reconfiguration of water around ion is given from the classical simulation of the autocorrelation function of the fluctuation of the angle j. The slow autocorrelation time was found to be 0.89 ps. The calculated time constant is similar to the slow decay time of 1.13 ps for the auto and cross correlation functions of the frequency fluctuations given in Table 2. Both the simulation and experiment are shown in Figure 11b. In the experimental fits the fast component of the frequency-frequency correlation function was assumed to be a delta function: the simulation gives a fast time constant of 27 fs. It is concluded that the observed frequency correlation functions are determined by hydrogen bond making and breaking around the perimeter of $DGdm^+$ causing a wagging of the -ND_2 groups. It is evident from the MD simulation that the -NH_2 groups are bending out of plane and wagging in response to their interactions with the water molecules. It was confirmed by computations that the frequencies of the degenerate mode components are strongly correlated with the configurations of the -NH_2 groups. Ab initio calculations on $[C(ND_2)_3]^+/D_2O$ clusters with up to 8 D_2O molecules showed that the degenerate mode near 1600 cm^{-1} can split by up to 80 cm^{-1} due to the interactions with asymmetrically disposed water molecules through H-bonding to the -ND_2 groups [30].

CONCLUSION

The 2D IR photon echo spectroscopy of the nearly degenerate asymmetric stretch vibrations of $DGdm^+$ in D_2O and D-glycerol/D_2O having perpendicular transition dipole moments showed an ultrafast growth of the cross peak between the two modes. Vibrational coupling of the two modes due to the system-bath interaction causes the population transfer (energy transfer) between them and also transfer between the inter-mode coherences which does not significantly contribute to the signal. A decay of the frequency-frequency correlation function

occurs on two timescales: a motionally narrowed limit which is presumed to be caused by fast (50 fs) librations of water molecules in the solvation shell; and a slower decay on the time scale of one picosecond which is determined by solvation shell reconfiguration including H-bond making and breaking around the ND_2 groups on the perimeter of $DGdm^+$.

Acknowledgments

This research was supported by grants to RMH from NSF-CHE and R01-NIH-GM12592 with instrumentation developed under PO1- NIH-RR001348.

REFERENCES

1. Jackson SE, Elmasry N, Fersht AR. Structure of the Hydrophobic Core in the Transition-State for Folding of Chymotrypsin Inhibitor-2 - a Critical Test of the Protein Engineering Method of Analysis. Biochemistry 1993;32(42):11270–11278. [PubMed: 8218192]
2. Mayo SL, Baldwin RL. Guanidinium Chloride Induction of Partial Unfolding in Amide Proton-Exchange in Rnase-A. Science 1993;262(5135):873–876. [PubMed: 8235609]
3. Bai YW, Sosnick TR, Mayne L, Englander SW. Protein-Folding Intermediates -Native-State Hydrogen-Exchange. Science 1995;269(5221):192–197. [PubMed: 7618079]
4. Wetlaufer DB, Coffin RL, Malik SK, Stoller L. Nonpolar Group Participation in Denaturation of Proteins by Urea and Guanidinium Salts . Model Compound Studies. J. Am. Chem. Soc 1964;86(3): 508–514.
5. Bello J, Haas D, Bello HR. Interactions of Protein-Denaturing Salts with Model Amides. Biochemistry 1966;5(8):2539–&. [PubMed: 4290986]
6. Moglich A, Krieger F, Kiefhaber T. Molecular basis for the effect of urea and guanidinium chloride on the dynamics of unfolded polypeptide chains. J. Mol. Biol 2005;345(1):153–162. [PubMed: 15567418]
7. Scott JN, Nucci NV, Vanderkooi JM. Changes in Water Structure Induced by the Guanidinium Cation and Implications for Protein Denaturation. J. Phys. Chem. A 2008;112(43):10939–10948. [PubMed: 18839935]
8. Magalhaes AL, Gomes JANF. Density-Functional Methods for the Study of the Ground-State Vibrations of the Guanidinium Ion. Int. J. Quantum Chem 1997;61:725–739.
9. Drozd M. Molecular structure and infrared spectra of guanidinium cation - A combined theoretical and spectroscopic study. Materials Science and Engineering B-Solid State Materials for Advanced Technology 2007;136(1):20–28.
10. Kim YS, Hochstrasser RM. Applications of 2D IR spectroscopy to peptides, proteins, and hydrogen-bond dynamics. J. Phys. Chem. B 2009;113(24):8231–51. [PubMed: 19351162]
11. Kuo CH, Vorobyev DY, Chen JX, Hochstrasser RM. Correlation of the vibrations of the aqueous azide ion with the O-H modes of bound water molecules. J. Phys. Chem. B 2007;111(50):14028–14033. [PubMed: 18044873]
12. Kuo CH, Hochstrasser RM. Two dimensional infrared spectroscopy and relaxation of aqueous cyanide. Chem. Phys 2007;341(1–3):21–28.
13. Kim YS, Wang JP, Hochstrasser RM. Two-dimensional infrared spectroscopy of the alanine dipeptide in aqueous solution. J. Phys. Chem. B 2005;109(15):7511–7521. [PubMed: 16851862]
14. Torii H, Tasumi M. Model-Calculations on the Amide-I Infrared Bands of Globular-Proteins. J. Chem. Phys 1992;96(5):3379–3387.
15. Schweitzer-Stenner R, Eker F, Griebenow K, Cao XL, Nafie LA. The conformation of tetraalanine in water determined by polarized raman, FT-IR, and VCD spectroscopy. J. Am. Chem. Soc 2004;126 (9):2768–2776. [PubMed: 14995194]
16. Lim M, Hochstrasser RM. Unusual vibrational dynamics of the acetic acid dimer. J. Chem. Phys 2001;115(16):7629–7643.
17. DeFlores LP, Ganim Z, Nicodemus RA, Tokmakoff A. Amide I `−II ' 2D IR Spectroscopy Provides Enhanced Protein Secondary Structural Sensitivity. J. Am. Chem. Soc 2009;131(9):3385–3391. [PubMed: 19256572]

18. Rubtsov IV, Wang J, Hochstrasser RM. Dual frequency 2D-IR of peptide amide-A and amide-I modes. J. Chem. Phys 2003;118(17):7733–7736.
19. Rubtsov IV, Wang JP, Hochstrasser RM. Dual-frequency 2D-IR spectroscopy heterodyned photon echo of the peptide bond. Proc. Natl. Acad. Sci. U. S. A 2003;100(10):5601–5606. [PubMed: 12709595]
20. Kurochkin DV, Naraharisetty SRG, Rubtsov IV. Dual-frequency 2D IR on interaction of weak and strong IR modes. J. Phys. Chem. A 2005;109(48):10799–10802. [PubMed: 16331922]
21. Cho MH. Coherent two-dimensional optical spectroscopy. Chem. Rev 2008;108(4):1331–1418. [PubMed: 18363410]
22. Piryatinski A, Tretiak S, Chernyak V, Mukamel S. Simulations of two-dimensional femtosecond infrared photon echoes of glycine dipeptide. J. Raman Spectrosc 2000;31(1–2):125–135.
23. Woutersen S, Hamm P. Structure determination of trialanine in water using polarization sensitive two-dimensional vibrational spectroscopy. J. Phys. Chem. B 2000;104(47):11316–11320.
24. Sando GM, Zhong Q, Owrutsky JC. Vibrational and rotational dynamics of cyanoferrates in solution. J. Chem. Phys 2004;121(5):2158–2168. [PubMed: 15260770]
25. Khalil M, Demirdoven N, Tokmakoff A. Vibrational coherence transfer characterized with Fourier-transform 2D IR spectroscopy. J. Chem. Phys 2004;121(1):362–373. [PubMed: 15260555]
26. Cahoon JF, Sawyer KR, Schlegel JP, Harris CB. Determining transition-state geometries in liquids using 2D-IR. Science 2008;319(5871):1820–1823. [PubMed: 18369145]
27. Kurochkin DV, Naraharisetty SRG, Rubtsov IV. A relaxation-assisted 2D IR spectroscopy method. Proc. Natl. Acad. Sci. U. S. A 2007;104(36):14209–14214. [PubMed: 17557837]
28. Tokmakoff A, Fayer MD. Homogeneous Vibrational Dynamics and Inhomogeneous Broadening in Glass-Forming Liquids - Infrared Photon-Echo Experiments from Room-Temperature to 10 K. J. Chem. Phys 1995;103(8):2810–2826.
29. Tokmakoff A, Urdahl RS, Zimdars D, Francis RS, Kwok AS, Fayer MD. Vibrational Spectral Diffusion and Population-Dynamics in a Glass-Forming Liquid - Variable Bandwidth Picosecond Infrared-Spectroscopy. J. Chem. Phys 1995;102(10):3919–3931.
30. Vorobyev DY, Kuo C-H, Chen J-X, Kuroda DG, Scott JN, Vanderkooi JM, Hochstrasser RM. 2D IR photon echo spectroscopy of guanidinium chloride. J. Phys. Chem. B. 2009 submitted.
31. Segur JB, Oberstar HE. Viscosity of Glycerol and Its Aqueous Solutions. Industrial and Engineering Chemistry 1951;43(9):2117–2120.
32. Kim YS, Hochstrasser RM. Dynamics of amide-I modes of the alanine dipeptide in D2O. J. Phys. Chem. B 2005;109(14):6884–6891. [PubMed: 16851775]
33. Hochstrasser RM. Two-dimensional IR-spectroscopy: polarization anisotropy effects. Chem. Phys 2001;266(2–3):273–284.
34. Ge NH, Zanni MT, Hochstrasser RM. Effects of vibrational frequency correlations on two-dimensional infrared spectra. J. Phys. Chem. A 2002;106(6):962–972.
35. Mukamel, S. Principles of nonlinear optical spectroscopy. Oxford University Press; New York: 1995. p. xviiip. 543
36. Redfield, AG. The theory of relaxation processes. In: Waugh, JS., editor. Advances in magnetic resonance. Vol. 1. Academic Press; New York: 1965. p. 1-32.
37. Phillips JC, Braun R, Wang W, Gumbart J, Tajkhorshid E, Villa E, Chipot C, Skeel RD, Kale L, Schulten K. Scalable molecular dynamics with NAMD. J. Comput. Chem 2005;26(16):1781–1802. [PubMed: 16222654]

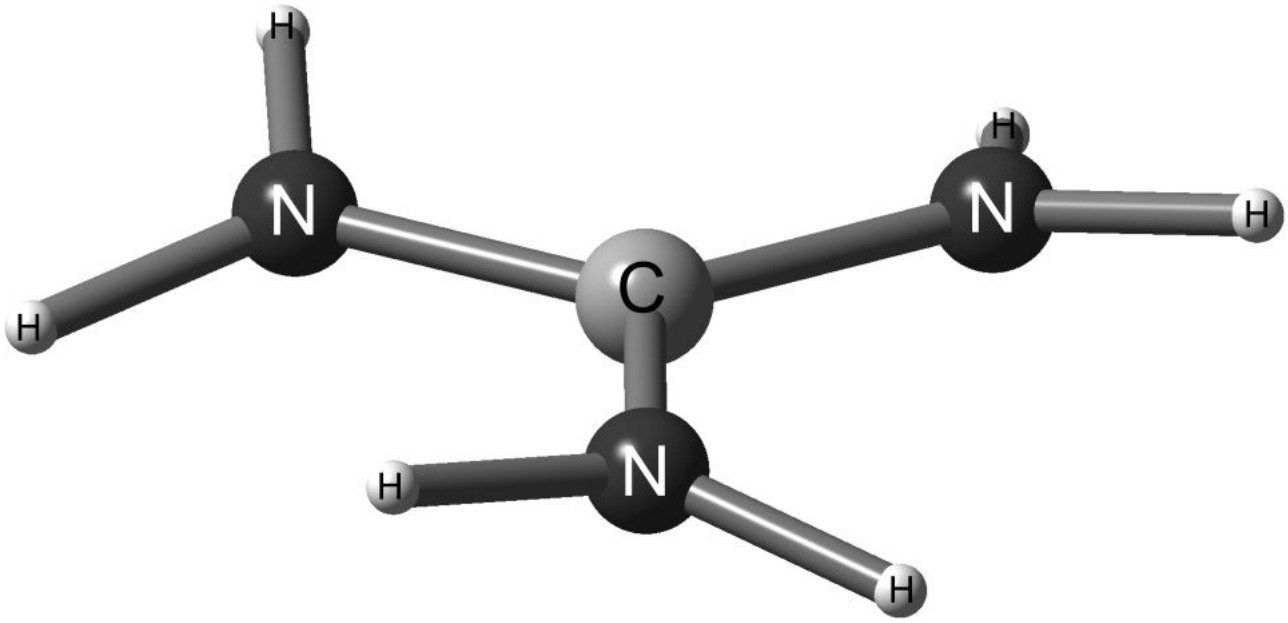

Figure 1. Structure of Gdm^+ in vacuum

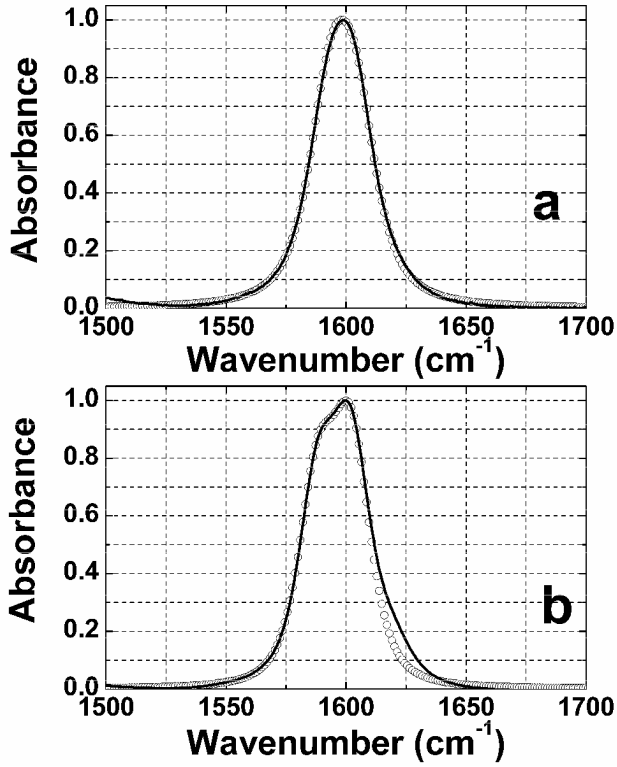

Figure 2. Linear FTIR spectra of guanidinium chloride

The normalized FTIR spectra of guanidinium chloride, $DGdm^+$, in **(a)** D_2O and **(b)** 59% D-glycerol/D_2O, after solvent absorption is subtracted. The circles represent the simulation of the linear FTIR spectra with parameters given in Table 2.

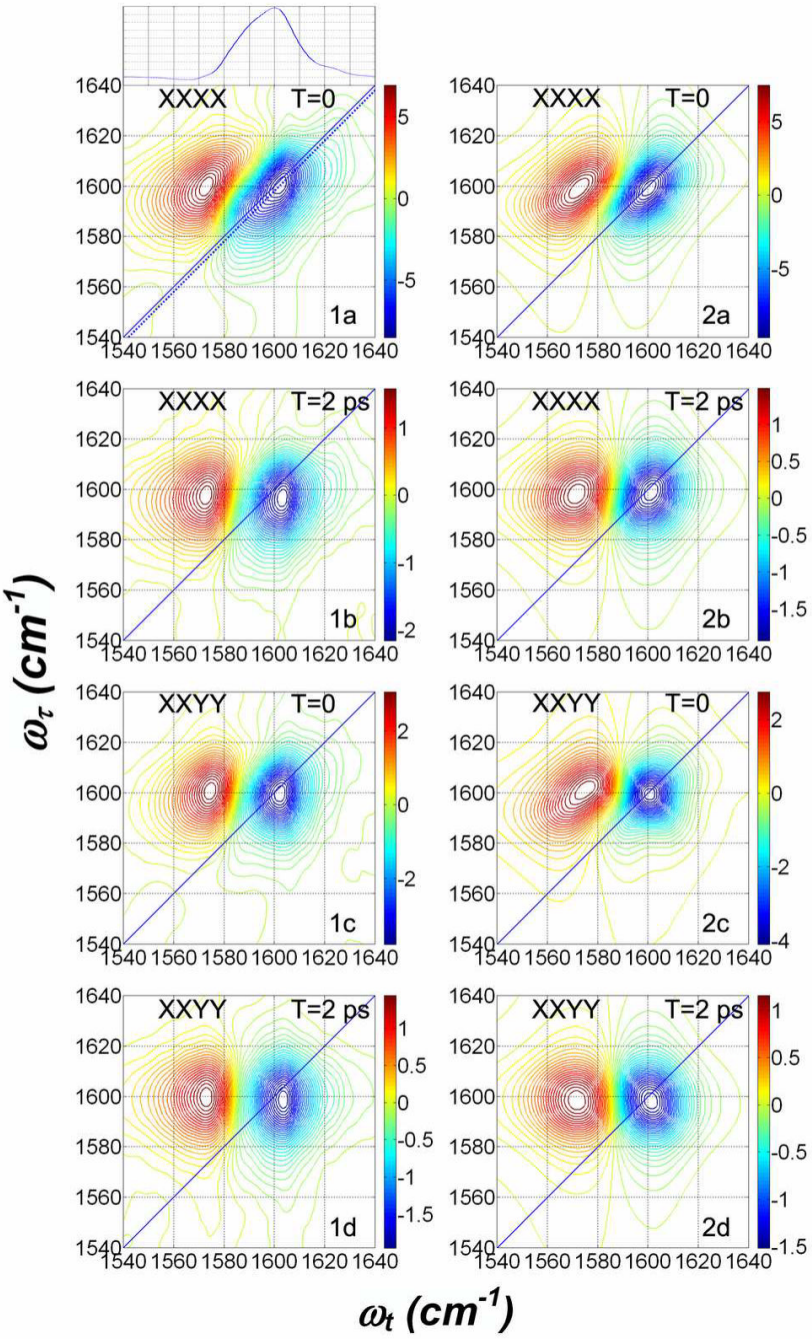

Figure 3. Polarization dependent absorptive spectra of 0.1 M DGdm$^+$ in D_2O

Experimental spectra (1a–1d) at the two indicated waiting times, T. Simulation results (2a–2d) with parameters from Table 2. The plot situated above (1a) is the trace along the dotted diagonal line shown in (1a). The polarizations of the pulses are indicated on each subplot.

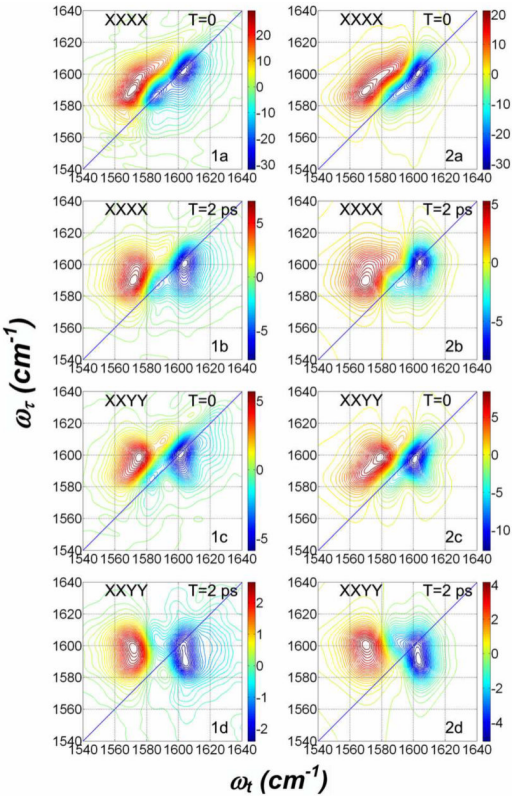

Figure 4. Polarization dependent absorptive spectra of 0.133 M DGdm$^+$ in 59% D-glycerol/D_2O
Experimental spectra (1a–1d) at the two indicated waiting times, T. Simulation results (2a–2d) with parameters from Table 2. The polarizations of the pulses are indicated on each subplot.

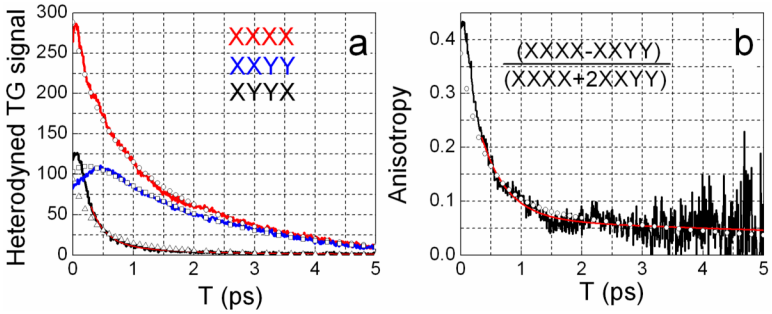

Figure 5. Heterodyned Transient Grating (TG) of $DGdm^+$ in D_2O

(a) Three tensor components of the experimental (red, blue and black curves) and simulated (circles, squares and triangles) heterodyned TG signals XXXX, XXYY and XYYX are shown. The signals are recorded at the maximum of the photoinduced absorption (1575 cm^{-1}). The smooth red curve almost coincident with the black curve for XYYX is a single exponential decay.

The simulation used parameters from Table 2 with ω_1= 1593.1 cm^{-1}, ω_2= 1604.5 cm^{-1}, Δ = 1.6 ps^{-1}, and k_{et}=1.1 ps^{-1} for the best fits.

(b) Anisotropy decay of $DGdm^+$ in D_2O from the TG measurement XXXX and XXYY. Experimental (black), the double exponential decay fit (red) and simulated (circles) anisotropy probed at the maximum of photoinduced absorption (1575 cm^{-1}).

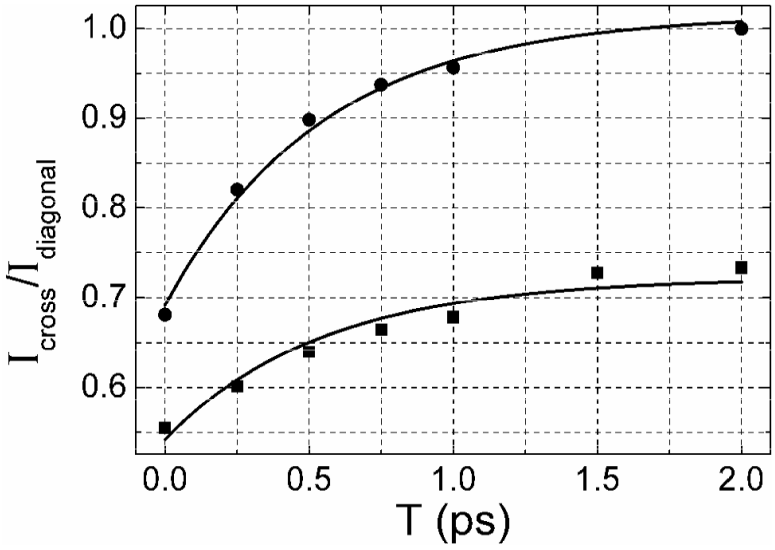

Figure 6. Cross peak dynamics

The ratio of the amplitudes between the cross peak at ω_τ = 1585 cm^{-1} and the diagonal peak at ω_τ = 1601 cm^{-1}, both at ω_τ =1601 cm^{-1}. The polarizations are XXXX (squares) and XXYY (circles). The data refer to the 2D IR absorptive spectra of 0.133 M $DGdm^+$ in 59% D-glycerol/D_2O. Single exponential fits (as discussed in the text) are shown as solid curves.

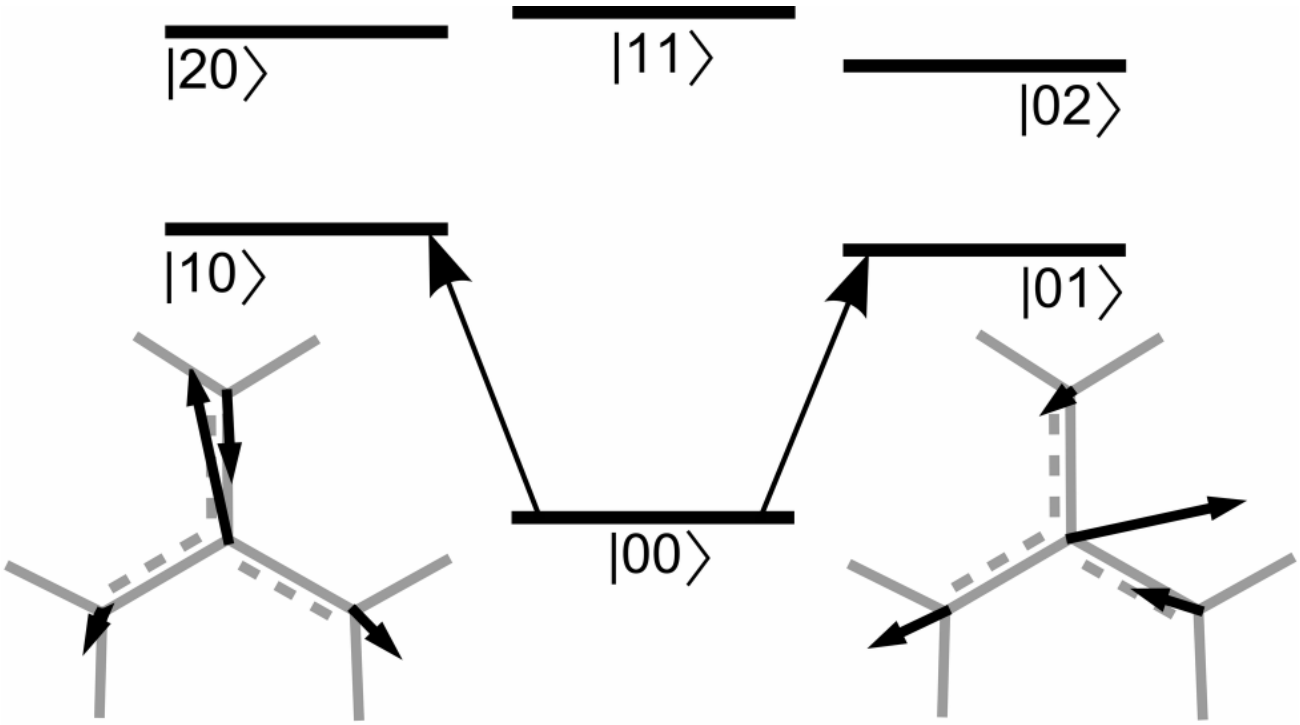

Figure 7. Energy diagram for the separated normal modes model

The displacements of the atoms of the CN_3 group of $DGdm^+$ for the two degenerate components of the 1600 cm^{-1} normal mode are shown. The atomic displacements illustrate the orthogonal polarization of the two transitions.

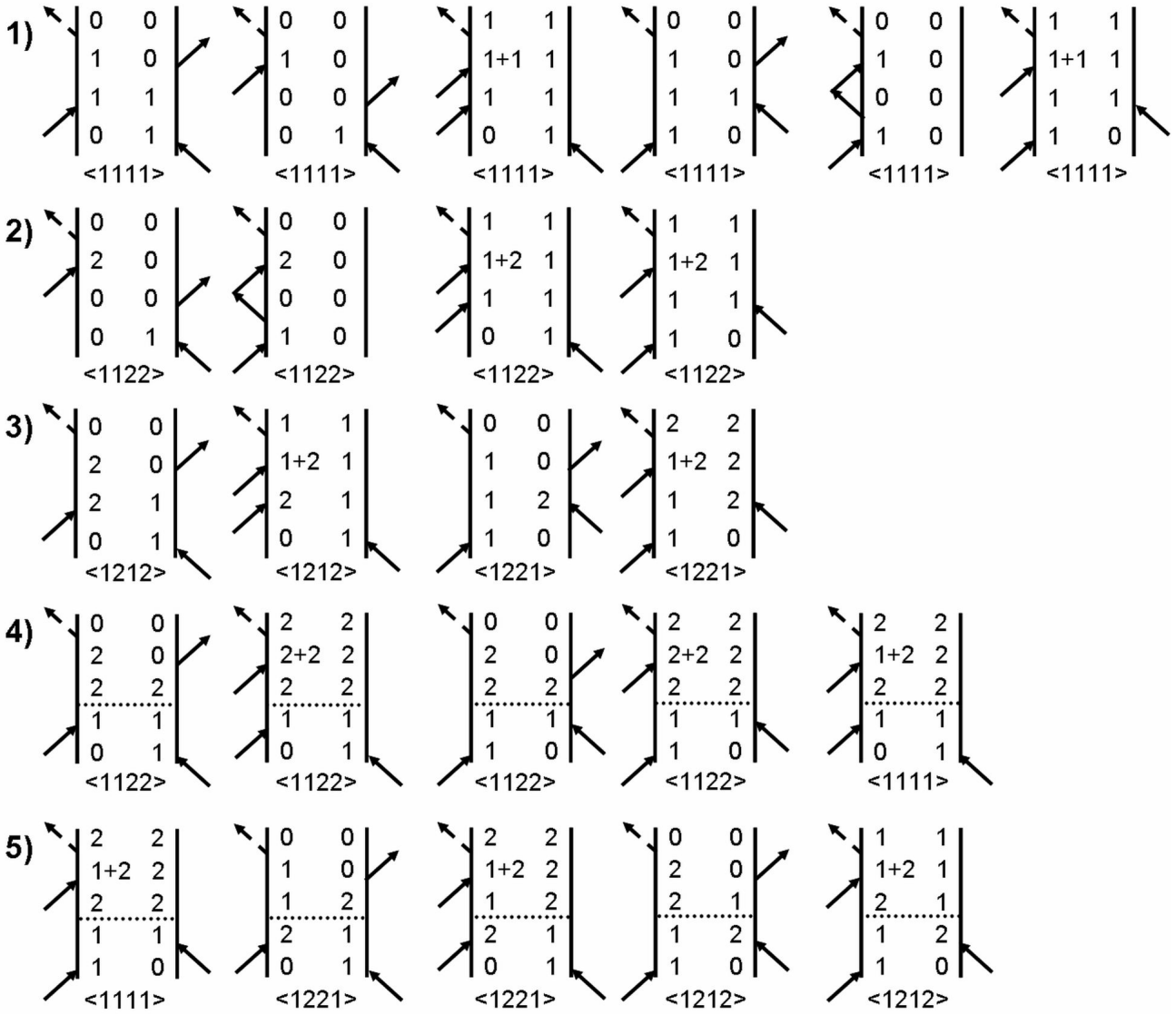

Figure 8. Liouville path diagrams for the photon echo signal emmited in the $-\vec{k}_1+\vec{k}_2+\vec{k}_3$ direction

Rows 1 and 2 describe stimulated emission (population of state 1 during waiting time), ground state bleaching (ground state 0 during waiting time) and excited state absorption (coherence of 1+1 or 1+2 states and state 1 after the third interaction). Row 3 describes diagrams with interstate coherence during the waiting time. Rows 4–5 describe population and coherence transfer between modes during T due to the system-bath interaction. The horizontal dashed line implies that a spontaneous process occurs in the indicated interval. The complete set of diagrams needed for simulations includes those with indices 1 and 2 interchanged.

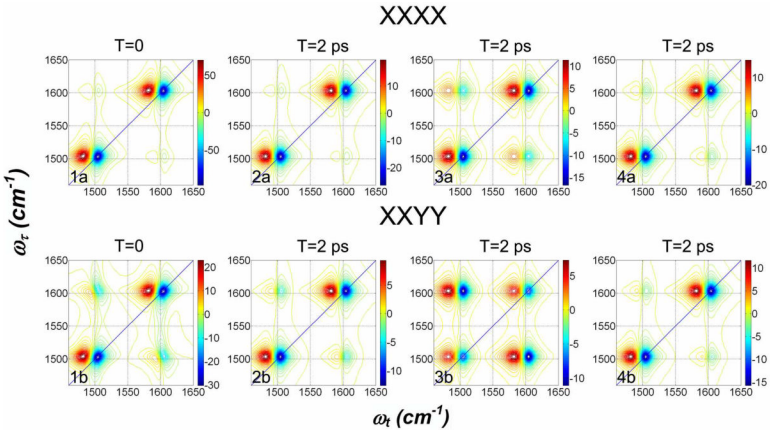

Figure 9. Simulated spectra for an artificially large (100 cm^{-1}) splitting of the degeneracy: effects of population exchange and 2π / 3 flips of the transition dipoles

The parameters are from Table 2 for $DGdm^+$ in D_2O. The upper row is for XXXX and the lower row for XXYY polarization.

1a and 1b: T=0, spectral diffusion incorporated, no population exchange or 2π / 3 flips.

2a and 2b: T=2 ps, otherwise as in 1a and 1b.

3a and 3b: T=2 ps, spectral diffusion and population exchange incorporated, no 2π / 3 flips.

4a and 4b: T=2 ps, spectral diffusion and 2π / 3 flips incorporated, but no population exchange.

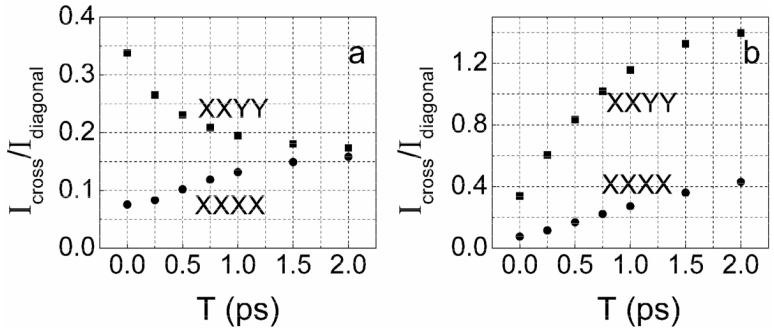

Figure 10. Simulated time dependence of the ratios of cross and diagonal peak intensities

Simulated 2D IR absorptive spectra for XXXX (circles) and XXYY (squares) polarizations with the assumption of **(a)** $2\pi / 3$ flips (as defined in the text) and no population exchange and **(b)** population exchange and no $2\pi / 3$ flips between component states.

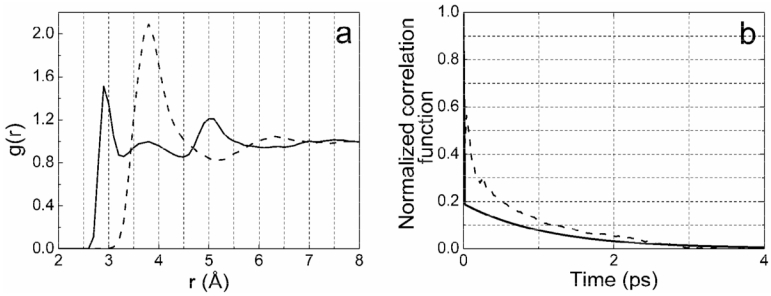

Figure 11. MD simulation results for Gdm^+ in H_2O

(a) Radial distribution functions $g_{NOw}(r)$ (solid curve) and $g_{COw}(r)$ (dashed curve) obtained from MD simulation of Gdm^+ in H_2O where O_w refers to a water oxygen atom. **(b)** Simulated (dashed curve) and experimental (solid curve) correlation decays. The simulation corresponds to $\langle \delta\varphi(t)\delta\varphi(0)\rangle/\langle \delta\varphi^2\rangle$ where $\delta\varphi$ is the fluctuation in the NH_2 wagging coordinate φ discussed in text. The experiment is the frequency-frequency correlation function with parameters given in Table 2 for $DGdm^+$.

Table 1

a) Orientational coefficients for Feynman paths for an oblate symmetric diffuser having two vibrational transition dipole moments in a plane perpendicular to the symmetry axis and **b)** The orientational factors for ±2π/3 flips.

a)

Tensor $*e^{2D(t+\tau)}$	**Feynman path (α β γ δ)**			
	(*iiii*)	(*ijij*)	(*iijj*)	(*ijji*)
$\langle X_\alpha X_\beta Y_\gamma Y_\delta \rangle$	$\frac{1}{45}\left[5 - 2e^{-6DT}\right]$	$-\frac{1}{30}e^{-6DT}$	$\frac{1}{45}\left[5 + 2e^{-6DT}\right]$	$\langle X_1 X_2 Y_1 Y_2 \rangle$
$\langle X_\alpha X_\beta X_\gamma X_\delta \rangle$	$\frac{1}{45}\left[5 + 4e^{-6DT}\right]$	$\frac{1}{15}e^{-6DT}$	$\frac{1}{45}\left[5 - 2e^{-6DT}\right]$	$\langle X_1 X_2 Y_1 Y_2 \rangle$

b)

$\left\langle X_\alpha^{A1} X_\beta^{A1} Y_\gamma^{A1} Y_\delta^{A1} \right\rangle$	1/15	−1/30	2/15	−1/30
$\left\langle X_\alpha^{A1} X_\beta^{A1} Y_\gamma^{A2} Y_\delta^{A2} \right\rangle = \left\langle X_\alpha^{A1} X_\beta^{A1} Y_\gamma^{A3} Y_\delta^{A3} \right\rangle$	7/60	1/60	1/12	1/60
$\left\langle X_\alpha^{A1} X_\beta^{A1} X_\gamma^{A1} X_\delta^{A1} \right\rangle$	1/5	1/15	1/15	1/15
$\left\langle X_\alpha^{A1} X_\beta^{A1} X_\gamma^{A2} X_\delta^{A2} \right\rangle = \left\langle X_\alpha^{A1} X_\beta^{A1} X_\gamma^{A3} X_\delta^{A3} \right\rangle$	1/10	−1/30	1/6	−1/30

Table 2

Parameters used for simulation of polarization dependent 2D IR absorptive spectra and linear FTIR spectra of $DGdm^+$ in D_2O and 59%D-glycerol/D_2O.

Parameters		Solvent	
		D_2O	**59% D-glycerol/D_2O**
ω_1, cm^{-1}		1593.0	1588.0
ω_2, cm^{-1}		1603.7	1602.3
Δ_1, cm^{-1}		25	18 ± 1
Δ_2, cm^{-1}		25	11 ± 1
Δ_c, cm^{-1}		5 ± 1	5 ± 1
$D_{\parallel}$, $D_{\perp}$, $*10^{-10}$ s^{-1}		3.3	0.33
μ_1/μ_2		1	0.905
k_{et}, ps^{-1}		0.53	0.71
$\langle\delta\omega_i(\tau)\delta\omega_i(0)\rangle$	γ, ps^{-1}	0.84	0.51
	Δ, ps^{-1}	2.0±0.4	1.45±0.15
	τ, ps	1.13±0.88	1.5±0.5